Selective excitation of localized surface plasmons by structured light

IGOR A LITVIN,[1,2] **NICLAS S MUELLER,**[1] **AND STEPHANIE REICH**[1,3]

[1]*Institut für Experimental Physik, Freie Universität Berlin, 14195 Berlin, Germany*
[2]*ilitvin@physik.fu-berlin.de*
[3]*reich@physik.fu-berlin.de*

Abstract: We investigated the selective excitation of localized surface plasmons by structured light. We derive selection rules using group theory and propose a fitting integral to quantify the contribution of the eigenmodes to the absorption spectra. Based on the result we investigate three nano oligomers of different symmetry (trimer, quadrumer, and hexamer) in detail using finite-difference time-domain simulations. We show that by controlling the incident light polarization and phase pattern we are able to control the absorption and scattering spectra. Additionally, we demonstrate that the fitting between the incident light and the oligomer modes may favor a number of modes to oscillate. Dark modes produce strong changes in the absorption spectrum and bright modes in the scattering spectrum. The experimental precision (axial shift error) may be on the same order as the oligomer diameter making the orbital angular momentum selection rules robust enough for experimental observation.

1. Introduction

The localized surface plasmons of metallic nanostructures have been intensively investigated due to their unique potential in manipulating light at the nanometer scale [1,2]. Plasmons also produce strong, localized electromagnetic fields that enhance optical processes by many orders of magnitude [3]. The decay of plasmon modes creates excited (hot) charge carriers that may be exploited for catalyzing chemical reactions and for photovoltaics [2,4,5]. The various applications of plasmonics require a control over the excitation of plasmonic modes. Some plasmon modes are better for optical enhancement and others for producing hot carriers [6]. Based on their lifetime and dipole moment plasmonic modes are divided into bright and dark [7,8]. Bright modes have a net dipole moment. They are excited by far-field radiation (linear- or unpolarized light) and decay as reemitted photons on a time scale of ∼5 fs. The net dipole moment of dark plasmons vanishes. They have longer lifetimes (∼20 fs) because the emission of photons into the far field is strongly reduced [9,10]. The selective excitation of a given eigenmode in a plasmonic oligomer would be a powerful tool for manipulating the plasmon oscillation time, absorption and scattering cross section, hotspot position, frequency, and far-field electromagnetic radiation.

An emerging way of tailoring plasmonic excitations is light with a complex and inhomogeneous distribution of phase and polarisation (structured light). Examples are beams with orbital angular momentum (OAM), spin angular momentum (SAM), and cylindrical vector beams (CVB) [11]. Conversely, nanooligomers and metasurfaces were used to create structured light at the nanoscale [12,13]. The complex phase-polarization pattern of structured light was implemented in materials science to control the chirality of twisted metal nanostructures [14], in nonlinear optics to increase the efficiency of second harmonic generation [15], and in nanoscale low-power optical trapping to increase the trap stiffness [16]. A number of new effects were also observed, such as dichroism of a plasmonic nanostructure interacting with OAM beams [17], and a spin-Hall effect in the scattering of structured light from a plasmonic nanowire [18].

Up to now, the excitation of plasmon eigenmodes by structured light was examined on a case by case basis using numerical simulations of the absorption and scattering spectra. Structured

light beams were used for exciting dark and bright plasmons with a complex distribution of surface charge density in nanooligomers [2,19,20,21,22], gold tetramers surrounded by a gold nanodisk array [23], coupled nano antennas [24], concentric spirals [25], and a plasmonic coaxial nanoring [26]. The case-by-case approach, however, is inherently limited. To systematically tailor the excitation of a specific mode, we need selection rules and predictions on the absorption based on the mode eigenvectors.

In this work we study the excitation of nanooligomers by light beams with orbital- and spin angular momentum. We first derive selection rules using group theory and then apply them to three oligomers of different symmetry. To quantify the contribution of the eigenmodes to the absorption spectra, we develop a model to fit the plasmon mode temporally and spatially to the incident electromagnetic radiation. A given beam of structured light may simultaneously excite dark and bright modes in an oligomer. The dark mode then produces dramatic changes in the absorption spectrum and the bright mode in the scattering spectrum. An axial shift of the laser beam with respect to the oligomer center keeps the major features in the absorption and scattering spectra intact. The experimental precision (axial shift error) may be on the same order as the oligomer diameter making the OAM selection rules robust enough for experimental observation.

2. Method

We simulated the selective excitation of plasmonic modes by structured light with the finite-difference time-domain (FDTD) method, using the commercial software package Lumerical FDTD Solutions. We constructed a trimer, quadrumer and hexamer of gold nanodiscs (diameter $d = 100$ nm, gap size $a = 15$ nm, height $h = 40$ nm) (see Fig. 1(a)). The dimensions of the structures were chosen such that the size of the individual nanodisks is much smaller than the wavelength of the incident light, but the overall dimension of the oligomer (215 nm for the trimer, 260 nm for the quadrumer, and 325 nm for the hexamer) are a considerable fraction of the beam width ($w_0 = 800$ nm). We illuminated the oligomers by vector beams with OAM and SAM. The incident beam was simulated by an embedded scripting language in the FDTD software. The electric field profile of the vector beam that is emitted by the source was implemented as

$$E_j(x, y, \omega, \ t, \ l, \ \varphi_j^s) = E_j^0(x, y)\exp(i(\omega t + l \ arctan(y/x) + \varphi_j^s)), \tag{1}$$

where $j = x$ or y specifies the x and y component of the vector beam with electric field amplitude E_j^0; ω is the oscillation frequency; l is the OAM order (the topological charge); $\varphi_j^s = \pm\pi/2$ is the respective phase shift between the x and y components to produce circular polarization of left or right handedness (see Figs. 1(b)–1(d)) [27].

Simulations were performed with the experimentally obtained Johnson–Christy dielectric function of gold [28]. In our analysis we focused on oligomer modes with energies <2 eV because modes with higher eigenenergies are damped by interband transitions [29].

There are different theoretical approaches to expand the electromagnetic response of plasmonic nanostructures in terms of eigenmodes. These include a multipolar decomposition of the single nanoparticle plasmons [30–33] and the hybridization of different nanoparticle multipoles in oligomers [9,34–35]. Here we use group theory [31,35] and the boundary elements method (BEM) [34]. The selection rules for light with OAM and SAM were obtained with group theory, following standard procedures [36]. To quantitatively predict absorption intensities from the fitting integrals introduced below, we calculated the oligomer eigenmodes using the BEM with the MATLAB package MNPBEM [34,37]. We used the MNPBEM package to calculate the spatial distribution of the surface charge density for each eigenmode. The surface charge distributions of the plasmonic eigenmodes from BEM represent the charge distribution at the respective eigenenergies. From the charge density distribution, we calculated the electric near field of the eigenmodes. We extracted the component $j = x, y, z$ of the electric field strength $E_j(x,y,z)$ using
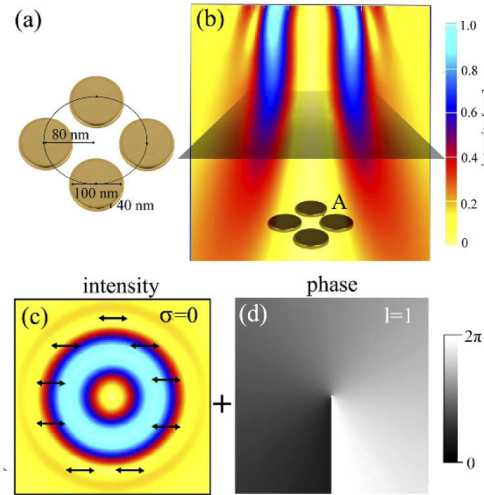
Fig. 1. (a) Geometry of the gold nanodisk quadrumer considered in this work. (b) Schematic of the excitation of plasmonic modes in a gold quadrumer with an orbital angular momentum (OAM) light beam ($l = 1$ and linearly polarized). (c) Intensity profile and (d) phase profile of the incident light beam.

Gauss law and the variable surface charge density field $\Delta q_j(x,y,z)$ [38]: $E_j(x,y,z) \sim \Delta q_j(x,y,z)/\Delta r_j$, where Δr_j is the distance between the points in the charge density distribution field.

3. Selection rules and fitting integral

To understand the selective excitation of plasmon eigenmodes for different light beams with orbital angular momentum, we analysed the selection rules considering the eigenvector of the plasmonic mode together with the beam profile. The key idea is that the incident field has to match the plasmonic eigenmode in frequency and space. One way to analyse this is through the symmetry transformation of the incoming field and the oligomer eigenmode. We consider plasmonic oligomers that consist of a regular geometric pattern of monomers with a horizontal mirror plane (σ_h), for example, nanoparticles and nanodiscs [39,40]. These oligomers belong to the D_{nh} point group, where n is the number of monomers in the oligomer (two for a dimer, three for a trimer, and so forth). In these point groups the representations may be specified by the following set of quantum numbers [41,42]: the component of the rotational momentum m along the z direction perpendicular to the horizontal mirror plane, the parity under the horizontal mirror plane σ_h and the vertical mirror plane σ_x. A beam with OAM transforms as follows in D_{nh}: for linear and circular polarization $\sigma_h = +1$ and σ_x is not defined. The m quantum number depends on the magnitude and relative orientation of the orbital l and spin σ momentums of the light beam $|m|=|l+\sigma|$. $\sigma = +1$ for left circular, -1 for right circular, and ± 1 for linear polarization due to an indeterminate oscillation direction of the unpolarized component; or alternatively because linearly polarized light can be understood as the sum of left and right circular polarization with equal weighting. Using these quantum numbers for a quadrumer (D_{4h} point group), the E_u representation is allowed for $l = 0$ and linear polarization as expected. Selected eigenvectors of the quadrumer are shown in Fig. 2. A beam with OAM $l = +1$ will excite modes of A_{1g} and A_{2g} symmetry for right circular polarization ($\sigma = -1$), whereas B_{1g} and B_{2g} modes are active under left circular polarization. The selection rules for $l=+1$ and linear polarization are $A_{1g} \oplus A_{2g} \oplus B_{1g} \oplus B_{2g}$.
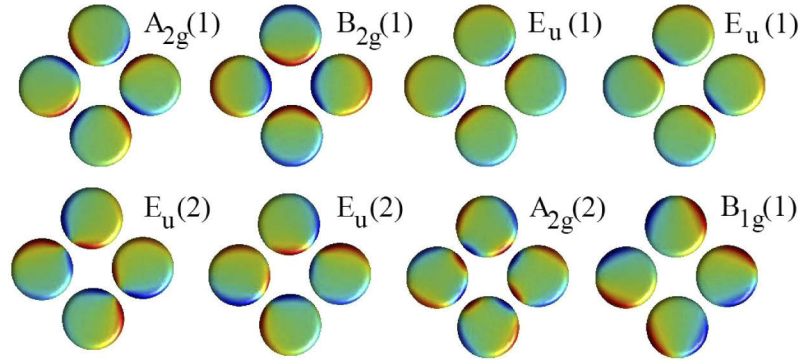
Fig. 2. Charge density plot of the lowest energy quadrumer eigenmodes obtained by boundary elements simulations. The eigenmodes are labeled by their symmetries within the D_{4h} point group of the quadrumer.

Table 1 summarizes the selection rules for beams with $l = 0$ and 1 in a trimer, quadrumer, and hexamer. In the point groups that contain the inversion symmetry (D_{4h} and D_{6h}), ungerade representations are excited for $l = 0$, but gerade for $l = +1$. Oligomers with higher n provide stronger spectral contrast between the allowed modes when varying l and σ. The rotational quantum number m in the D_{nh} point groups is only well defined for $|m| < n/2$. There is a set of Umklapp rules for larger m, e.g., $m' = n/2 - m$ for $n/2 < m < n$ [41,42]. For that reason, a total angular momentum $m = 2$ ($l = +1$, $\sigma = +1$) is identical to $m = 1$ ($l = 0$, $\sigma = \pm1$) in a trimer resulting in identical selection rules for $l = 0$ and a beam with $l = +1$ and left circular polarization.

Table 1. Optical selection rules for a trimer, quadrumer, and hexamer for different light beams.

OAM l	right circular ($\sigma = -1$)	left circular ($\sigma = +1$)	linear
trimer (D_{3h})			
0	E'	E'	E'
+1	A'$_1$ $\oplus$ A'$_2$	E'	A'$_1$ $\oplus$ A'$_2$ $\oplus$ E'
quadrumer (D_{4h})			
0	E_u	E_u	E_u
+1	$A_{1g} \oplus A_{2g}$	$B_{1g} \oplus B_{2g}$	$A_{1g} \oplus A_{2g} \oplus B_{1g} \oplus B_{2g}$
hexamer (D_{6h})			
0	E_{1u}	E_{1u}	E_{1u}
+1	$A_{1g} \oplus A_{2g}$	E_{2g}	$A_{1g} \oplus A_{2g} \oplus E_{2g}$

The symmetry analysis provides a *qualitative* yes/no answer to the question whether a particular plasmon mode gets excited by a given polarization and phase profile. We now propose a fitting integral that *quantifies* the answer. It tells us how strong a peak will appear in the absorption spectrum. For the efficient excitation of a mode in a metallic nanostructure the components of the incident electromagnetic field must match the electric field of the plasmon in space and time. The excitation efficiency of a mode is calculated from the maximum value of a fitting integral $F_i(\varphi_0)$ that describes the coupling of the incident beam to a specific mode [30,33]:

$$F_i(\varphi_0) = \int_0^T dt \iiint_V dr^3 \vec{M}_i(\vec{r}, t) \cdot \vec{E}(\vec{r}, t, \varphi_0) \Big/ \int_0^T dt \iiint_V dr^3 \left| \vec{E}(\vec{r}, t, \varphi_0) \right|^2 \qquad (2)$$

$\vec{M}_i(\vec{r}, t)$ is the electric field of the eigenmode i, $\vec{E}(\vec{r}, t, \varphi_0)$ (see Eq. (1)) the electric field of the incident beam, and φ_0 the phase delay between the incident field E and the field of the plasmon mode M_i. The integral must be taken over the volume V of the plasmonic nanostructure and an electromagnetic field oscillation period $T = 2\pi/\omega$ for the specific plasmon mode. The integral in Eq. (2) can be simplified for a range of incident electric field distributions and plasmon modes (see Appendix).

Based on Eq. (2) including the electric field distribution of the incident beam we calculate the excitation efficiency of the oligomer modes by a particular structured light beam [11]. We illustrate the action of the fitting integral for the A_{2g}, B_{1g}, and E_u modes of a quadrumer for a linearly polarized incoming beam with $l = +1$ (see Fig. 3) and for a beam with spin angular momentum (see Fig. 4). The electric field distribution of the beam is compared to the surface charge density and near field of the plasmonic modes. A beam with orbital angular momentum ($l = +1$) but no spin will excite the A_{2g} and B_{1g} mode, but not the E_u mode (Fig. 3). An angular momentum beam with spin will, selectively excite the A_{2g} mode for $\sigma = +1$ or the B_{1g} for $\sigma = -1$ (Fig. 4). This is because, both, the x and y component of the electric field must match the plasmonic mode in space and time.
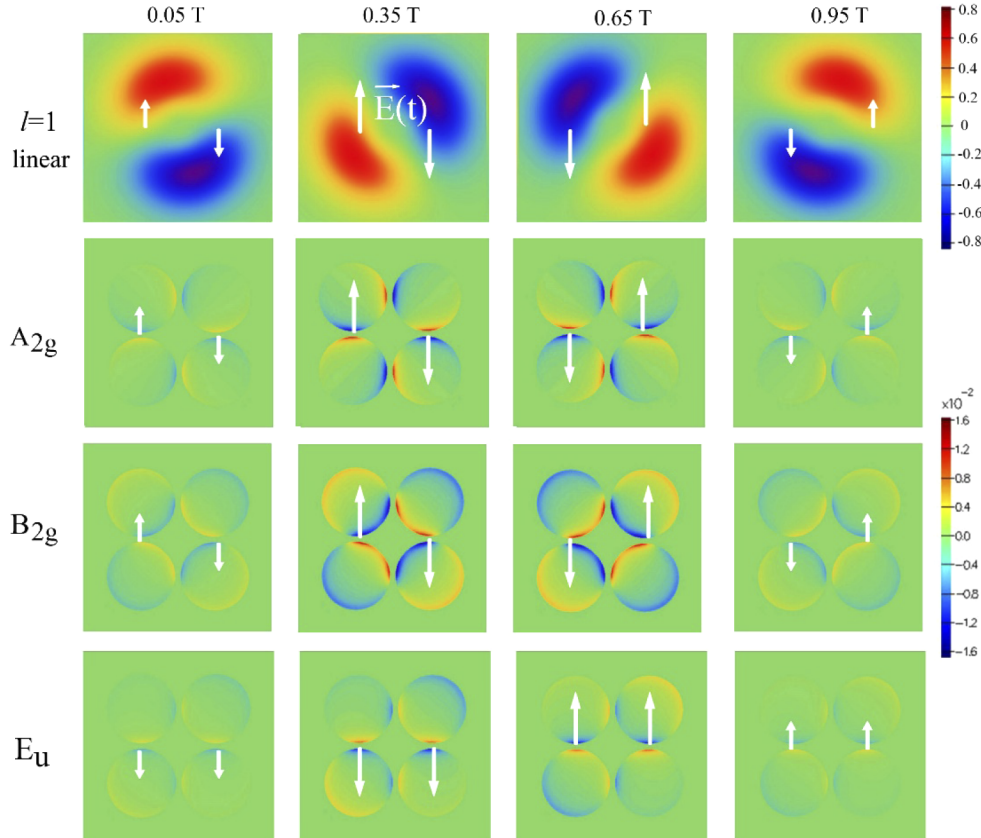

Fig. 3. Electric field distribution of a linearly polarized light beam with OAM shown at specific times over one oscillation period T (top row); oscillation of the surface charge density of the A_{2g} (second row), B_{2g} (third row), E_u (bottom row) modes over one period. White arrows show the direction of the electric field vector at the "hot spots" (bottom rows) and the incident beam (top row).
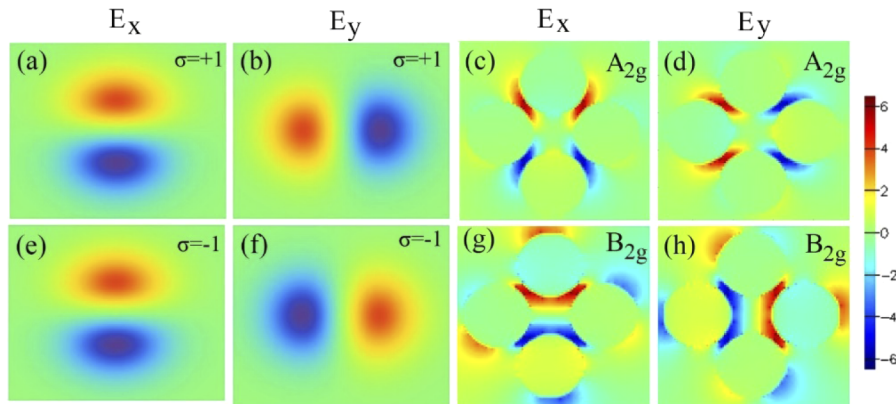
Fig. 4. The x (a, e) and y (b, f) components of the electric field vector of an incident light beam with OAM ($l = 1$) and SAM $\sigma = +1$ in (a, b) and $\sigma = -1$ in (e, f). It is compared to the electric near field of the plasmonic quadrumer modes A_{2g} (c, d) and B_{2g} (g, h) obtained from FDTD simulations.

4. Quadrumer

We apply the optical selection rules and the method of the fitting integral to a plasmonic quadrumer as a first exemplary structure. The absorption spectrum of the quadrumer differs fundamentally for excitation without ($l = 0$) and with OAM ($l = +1$) (see Figs. 5(a)–5(b)). Without OAM the simulation predicts a broad peak (full width at half maximum FWHM = 0.5 eV) at 1.7 eV. It occurs because of the absorption and scattering by the bright E_u mode. The spectrum changes fundamentally for $l = +1$ (see Fig. 5(b)). It consists now of two peaks at 1.56 eV (794 nm, Fig. 5(b)) and 1.79 eV (693 nm, Fig. 5(b)), and a broader feature above 2 eV. For assigning the plasmon eigenmodes, we extracted the surface charge densities (see Figs. 5(d)–5(f)) and respective vector plot of electric near field (see Figs. 5(c)–5(e)) at the frequencies of maximum intensity. The transformation properties identify the excited modes as A_{2g} (1.56 eV) and B_{2g}
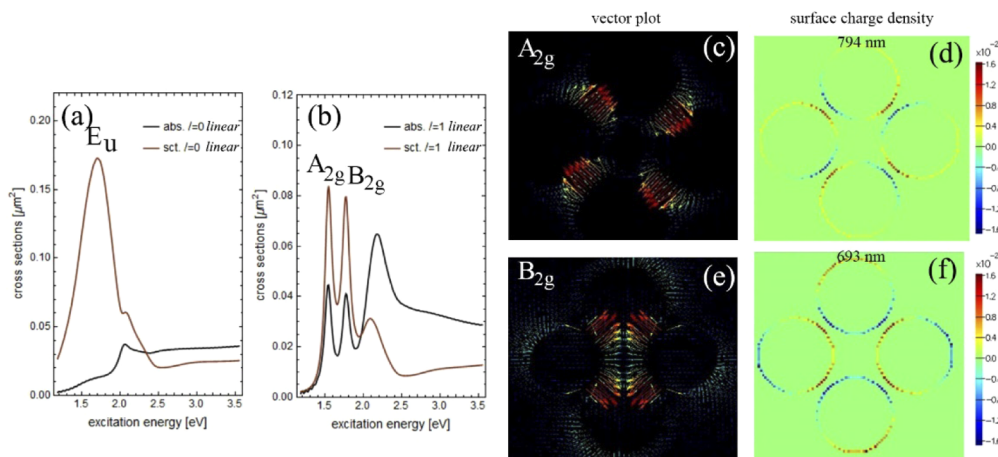

Fig. 5. (a) Absorption (black) and scattering (brown) cross section of a quadrumer excited with linearly polarized light and (b) linearly polarized light with OAM. Electric near field of the A_{2g} (c) and B_{2g} (e) modes and respective surface charge densities (d, f) obtained from FDTD simulations.

(1.79 eV), compare eigenmodes in Fig. 2, in excellent agreement with the group theory selection rules. These two modes have a vanishing net dipole moment and are considered optically inactive or dark.

To see the temporal behaviour of the excited modes, we analysed the oscillation of the total electric field in one of the hot spots between two discs (see point A in Fig. 1(b) For an OAM beam with $l = +1$ (linearly polarized), the oscillation of the field extends over 60 fs with an amplitude beating that comes from the interference of the two plasmonic modes (see Figs. 6(a)–6(c)). The long oscillation is the reason for the comparatively narrow line width in the absorption spectrum (see Fig. 5(b)). A_{2g} and B_{2g} modes have no net dipole moment and a long radiative lifetime. At the same time, material losses of gold are small below 2 eV (intrinsic line width <100 meV, [29]). Figures 5(c) and 5(e) shows the electric field distribution and Figs. 5(d) and 5(f) the surface charge density obtained from FDTD simulations at the frequencies of maximum absorption. The electric field- and charge distributions agree nicely with the $A_{2g}(1)$ and $B_{2g}(1)$ eigenmodes of the quadrumer in Fig. 2, confirming our symmetry assignment.
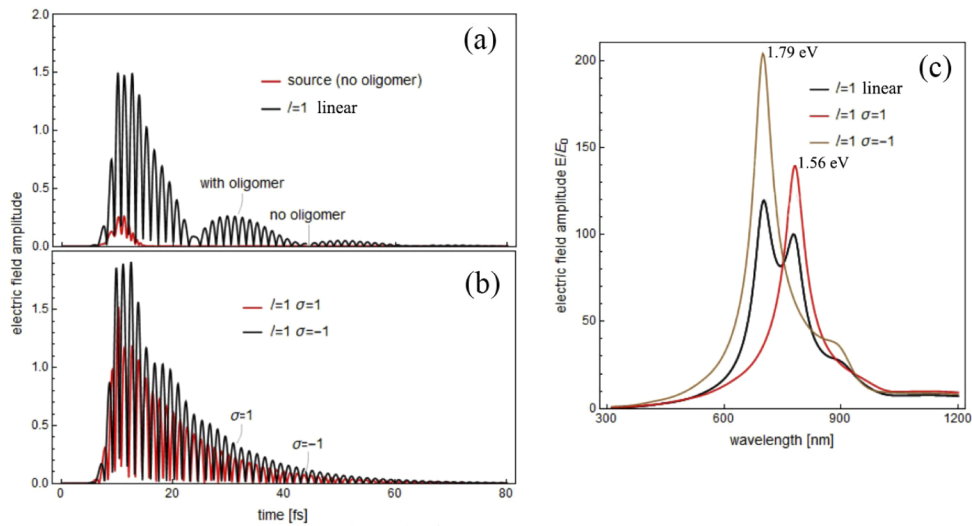

Fig. 6. (a) Oscillation of the electric near field amplitude at point A in Fig. 1(b) as a function of time, for a linearly polarized incident beam with OAM and (b) for an incident beam with OAM and SAM; (c) associated Fourier spectrum of the field oscillations in (a) and (b).

Adding spin angular momentum (SAM) to the incident beam results in more stringent selection rules for optical absorption than linear polarization (see Table 1). This is also discernible in the field and charge distribution of the eigenmodes. The fields of the $A_{2g}(1)$ and $B_{2g}(1)$ modes are identical along the horizontal axis (see x axes in Fig. 4). Perpendicular to it however, the fields have opposite sign over the entire oscillation period (see y axes Fig. 4). In other words, the excited quadrumer modes (A_{2g} and B_{2g}) are in phase in the horizontal direction and out of phase ($\Delta\varphi = \pi$) in the vertical direction (see Figs. 4(c)–4(h)). A similar behaviour of the electric field occurs for incident beams with opposite signs of the SAM, i.e. clockwise ($\sigma = -1$) or anticlockwise ($\sigma = +1$) rotation direction (see Figs. 4(a)–4(d)).

We simulated the optical spectra for an OAM light beam with SAM (see Figs. 7(a)–7(b)). The presence of the SAM in the incident light beam leads to the selective excitation of either the A_{2g} or the B_{2g} mode. Adjusting the phase shift between the two orthogonal polarization components of the incident beam controls the relative excitation efficiency of the two modes (see Figs. 7(a) and 7(b) and Fig. 6(c)). It strongly changes absorption and scattering, resulting in an SAM contrast between the spectra of the two modes. The spectral contrast may be used as a

detector for SAM and phase shift between the orthogonal electric vector components. A linearly polarized beam corresponds to the sum of two circularly polarized beams with opposite spin [11]. Therefore, the A_{2g} and B_{2g} modes are both excited for an OAM beam with linear polarization (see Fig. 5(b)).
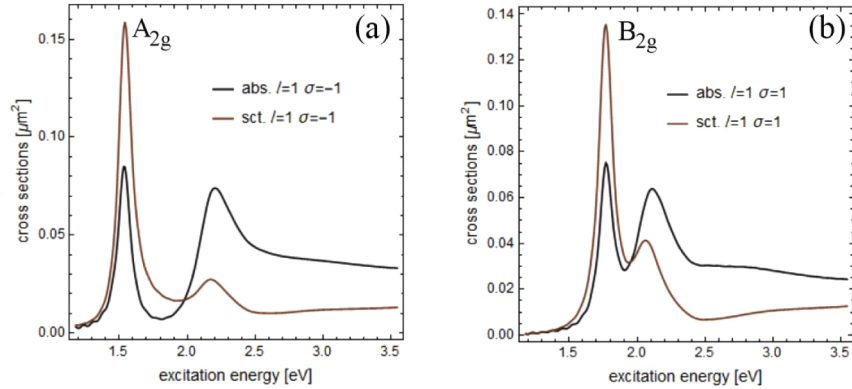

Fig. 7. Absorption and scattering cross-sections obtained by FDTD simulations for a quadrumer illuminated by OAM beams with (a) $l = 1$ and $\sigma = -1$, and (b) $l = 1$, and $\sigma = 1$.

We now predict the relative absorption intensities of the plasmonic modes using the fitting integral introduced in Eq. (2). The fitting integral is evaluated for the seven quadrumer modes with lowest energy and excitation with OAM light, with and without SAM (see Fig. 8(a)) at the eigenenergies of the respective plasmonic modes.
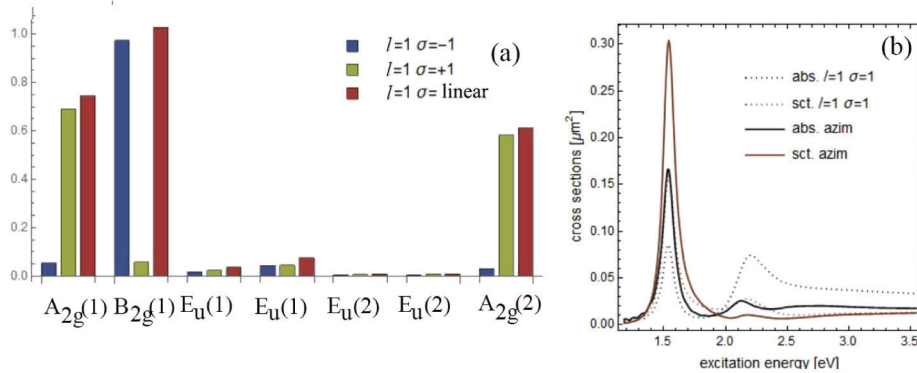

Fig. 8. (a) Normalized solutions of the fitting integral, Eq. (2), for incident beams with $l=1$, $\sigma=-1$ (blue); $l=1$ (linearly polarized) (red); $l=1$, $\sigma=+1$ (green) and 7 quadrumer modes with lowest energy eigenvalues (excitation energies below 2 eV). (b) Absorption and scattering cross-sections obtained by FDTD simulations of the quadrumer illuminated by a beam with OAM ($l=1$), SAM ($\sigma=-1$) (dashed) and with azimuthal polarization (solid).

The calculations for the B_{2g}, A_{2g}, and E_u modes excellently agree with the selection rules in Table 1 and the FDTD simulations in Figs. 5–7. In addition to the main peaks, the simulated spectra also contain peaks around 2.15 eV (580 nm). The fitting integral predicts absorption by another set of A_{2g} and B_{2g} modes in this region (see Fig. 8(a)). Due to the interband transitions of gold, the lifetime of these plasmon modes reduces to 4-6 fs. It leads to the broadening of the absorption spectra and a dramatic drop in the maximum of the scattering cross section peak (see Fig. 7(a), (b)). An additional reason for the broadening is the spectral overlap with the

neighbouring radial breathing mode A_{1g} [42] around 530 nm (2.34 eV), which is also excited by OAM light beams (see Table 1). For such geometry of the oligomer the lifetime of the radial breathing mode [43] is dramatically low (around 4-6 fs) due to high gold absorption in this spectral region and a quite high required excitation energy.

The fitting integral is also a great tool to optimize the excitation of a given mode. For example, the A_{2g} mode of the quadrumer may also be excited with azimuthal polarization of the incident beam (Fig. 8(b)). The fitting integral of the low-energy A_{2g} mode and azimuthally polarized light is much larger than for a beam with $l = +1$ and $\sigma = -1$. Absorption and scattering for azimuthally polarized light are more than twice as high as for excitation with an OAM light beam (see Fig. 8(b)).

5. Plasmonic Trimer and Hexamer

With the fitting integral, Eq. (2), we can quickly evaluate multiple plasmonic oligomers for the interaction with orbital angular momentum beams. We calculated the fitting integrals of a trimer and a hexamer for linearly polarized light with OAM ($l = +1$) and without OAM ($l = 0$) and right ($\sigma = -1$) and left ($\sigma = +1$) circular polarization. We considered all eigenmodes with an eigenenergy below 2 eV. Additionally, we determined the net dipole moment of the modes (bright or dark mode) from the fitting integral for linear polarization and $l = 0$. The fitting integrals (see Figs. 9(a) and 9(sd)) correctly predict the relative absorption and scattering spectra (see Figs. 9(b), 9(c), 9(e), and 9(f)) for incident beams with given OAM and SAM. Expectably, we see dramatic differences between bright and dark modes in the absorption and scattering spectra. The dark modes are most pronounced in the absorption spectra and the bright modes in the scattering spectra. This is in excellent agreement with the lifetime difference between dark and bright modes: The longer electromagnetic oscillations in the oligomer produce stronger dissipative
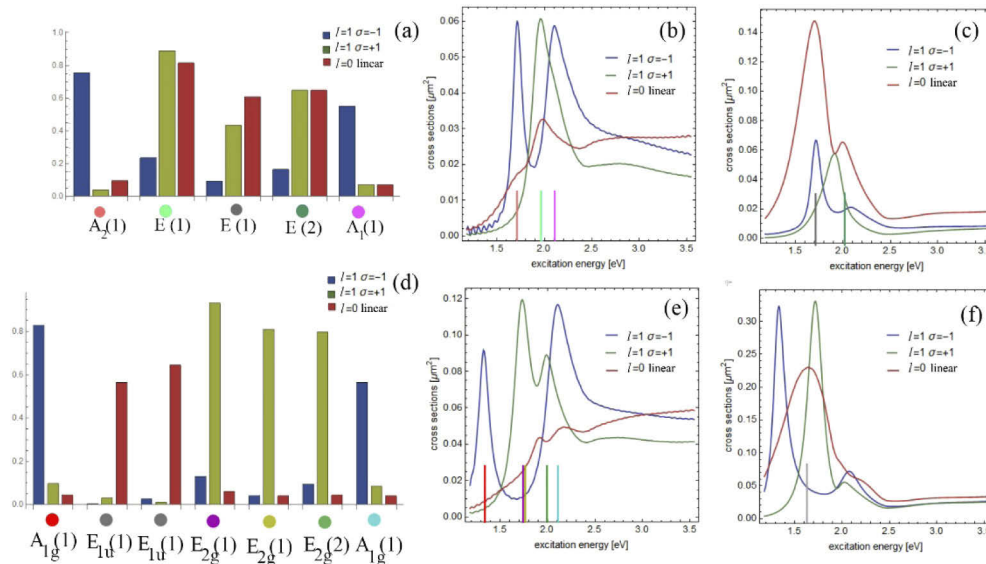

Fig. 9. Normalized solution of the fitting integral, Eq. (2), for the first five trimer modes (a) and seven hexamer modes (at the eigenenergies of the respective plasmonic modes) (d) with lowest eigenenergies below 2 eV for incident beams with OAM and SAM: $l=1$, $\sigma=+1$ (green); $l=1$, $\sigma=-1$ (blue); $l=0$, (linearly polarized) (red). (b) Absorption (b, e) and scattering (c, f) cross-sections obtained by FDTD simulations for a trimer (b,c) and hexamer (e,f) illuminated by beams with similar OAM and SAM.

energy absorption. The bright modes E'(1) and E'(2) with non-zero net dipole moment (see Fig. 9(a)) get excited by beams with OAM and SAM in the trimer, in contrast to the quadrumer. The reason is the lower order of the principle axis of rotation. In a trimer, the quantum number for the angular momentum can only take the values of zero and one, making the selection rules for $l + \sigma = +2$ identical to $l + = 0$ (see Table 1). A low order of the principle axis of rotation reduces the spectral contrast for different $|l + \sigma|$ and makes an oligomer less sensitive towards distinguishing between incident beams with different handedness (see Fig. 9(b)).

The excitation behaviour of hexamer plasmons is quite similar to the quadrumer. There is a strong modal discrimination for incident beams with different sign of the SAM (see Figs. 9(d)–9(f)). In contrast to the trimer, no bright modes are excited in the hexamer by a beam with $l = +1$. This is due to the six-fold principle axis of rotation in a hexamer. The fitting integrals excellently describe the absorption spectra by the oligomer (see Fig. 9(d)). Due to strong gold absorption in the spectral region above 2 eV we see a damping of the scattering cross section in this region.

6. Axial shift

Structured light has a varying polarization and/or phase profile across the light beam. It makes such beams much more sensitive towards shifts in the alignment compared to a linearly polarized Gaussian beam without OAM. To examine the possible experimental implementation of our results, we simulated the evolution of the absorption and scattering spectra with an axial shift of the incident beam, see Fig. 10(a). Again, this behaviour may be evaluated straightforwardly with the fitting integral. In Fig. 10(b) we show the changes in the fitting integral and in Figs. 10(d) and 10(e) the absorption and scattering spectra as a function of axial shift.

The bright modes $E_u(1)$ and $E_u(2)$ are symmetry forbidden for perfect alignment and had zero fitting integral for all OAM beams. The fitting integral for these modes gradually increases with the axial shift. This leads to a rise in the excitation efficiency of the E_u modes with misalignment, which we see in the absorption and scattering spectra (see Figs. 10(d) and 10(e)). The fitting integral for the dark modes decreases with axial shift, e.g., almost by a factor of two for the A_{2g} and the B_{2g} modes in Fig. 10(b). Surprisingly, an axial shift by the oligomer size away from the center ($\Delta x = 120$ nm, Fig. 10(a)), produces only little changes in the absorption and scattering spectra (see Figs. 10(d) and 10(e)). We are able to identify the oscillating modes and spectral behaviour of the excited oligomer after an axial beam shift that is comparable to the oligomer radius. This means that the experimental precision (the oligomer centre aiming by incident beam) has to be on the order of the oligomer diameter. Such a precision is achievable in experiments and opens the possibility for implementation in the fields of nano engineering and sensing.
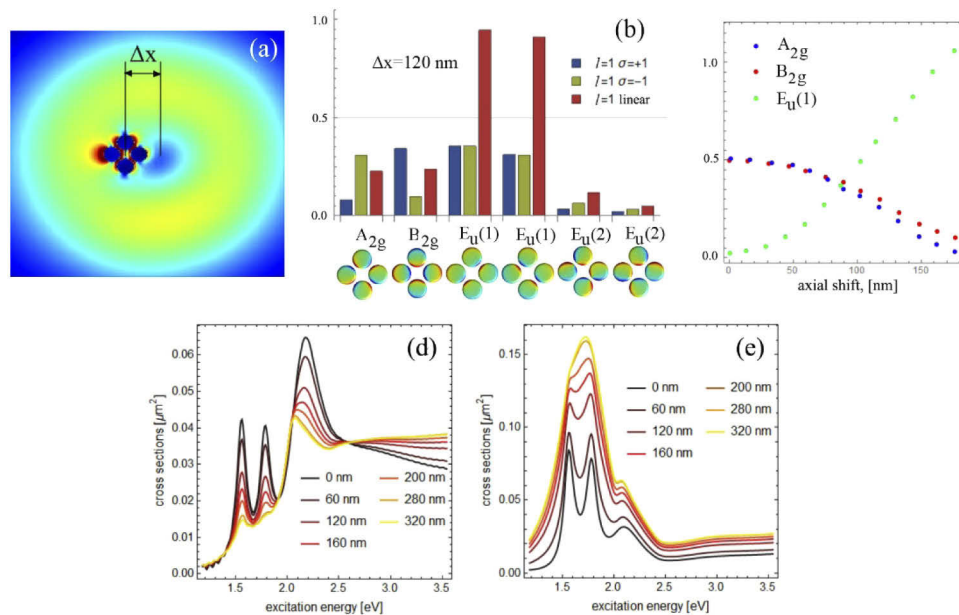
Fig. 10. (a) Electric field intensity as a function of position, obtained by FDTD simulations. The oligomer is shifted with respect to the beam center along the x axis. (b) Normalized solutions of the fitting integral, Eq. (2), for the first six quadrumer modes with lowest excitation energy below 2 eV. The incident beams with OAM and SAM are shifted by 120 nm from the oligomer inversion center. (c) Dependence of the fitting integral on the axial oligomer shift for the first three quadrumer modes and a linearly polarized beam with OAM. (d, e) Evolution of the absorption (d) and scattering (e) cross-sections obtained by FDTD simulations of the quadrumer illuminated by an axially shifted beam with OAM (l=1 and linearly polarized).

7. Conclusion

In this work we proposed how to selectively excite the localized surface plasmons of oligomers with cylindrically symmetric placed gold nanoparticles (nanodiscs) by structured light. The technique can be generalized to the excitation of oligomers with more complex geometry. To quantify the absorption by a particular eigenmode we developed a model to temporally and spatially fit the plasmon mode to the incident electromagnetic radiation (fitting integral). The method (fitting integral) excellently described the absorption and scattering spectra by the oligomer. Moreover, we applied group theory selection rules to three oligomers of different symmetry. We have shown that it is possible to use both the group theory selection rules and fitting integral to find the required incoming beam properties such as OAM and SAM to excite the specific dark or bright modes (and the absorption and scattering spectra) of the oligomer of chosen geometry. Additionally, we see that the technique described above can favour a number of modes to oscillate, however the oligomer material plays a dramatic role in the damping of the modes at large excitation energies. Dark modes are most pronounced in the absorption spectra and bright modes in the scattering spectra. This is in excellent agreement with the lifetime difference between dark and bright modes. We showed that a small axial shift of an OAM laser beam with respect to the oligomer center has only a minor effect on the absorption and scattering spectra. Namely, the experimental precision in beam alignment must be on the order of the oligomer diameter. Such a precision is achievable in experiments and opens the possibility for implementation in the fields of nano engineering and sensing.

Appendix

We are able to simplify the temporally dependent part of the fitting integral for most combinations of incident beam and plasmon eigenmodes. For a vanishing (or very small) z component of the plasmon eigenmode i we express $M_j^i(x, y, t) = M_j(x, y) \sin(\omega t)$ and $E_j(x, y, t, l, \alpha_j^s, \varphi_0) = E_j^0(x, y) \cos\left(\omega t + l \arctan\left(\frac{y}{x}\right) + \alpha_j^s \frac{\pi}{2} + \varphi_0\right)$, where $j = x, y$ specifies the x and y component of the electric field vector of the oligomer mode and the incident beam. α_j^s represents the polarization behaviour, for example, for linear polarization $\alpha_x^s = \alpha_y^s = 0$ and for circular polarization $\alpha_x^s = 0$ and $\alpha_y^s = \pm 1$ (the sign is responsible for the handedness). l is an integer that is responsible for the magnitude of OAM (the topological charge, $l\hbar$ - the energy per OAM carrying photon [44]). φ_0 is the phase shift between the incident light and the plasmon mode. We find

$$F_j^i(\varphi_0) = T_j(\varphi_0) \iint dxdy \, M_j^i(x, y) E_j^0(x, y) / \iint dxdy \, |E_j^0(x, y)|^2,$$

where

$$T_j(\varphi_0) = \sin\left(l \arctan(y/x) + \alpha_j^s \frac{\pi}{2} + \varphi_0\right).$$

The obtained integral is temporally independent and can simplify the integration. In the case of different frequencies between the oligomer plasmon and the incoming light, the temporally dependent part goes to zero.

Disclosures

The authors declare that there are no conflicts of interest related to this article.

References

1. J. A. Schuller, E. S. Barnard, W. Cai, Y. C. Jun, J. S. White, and M. L. Brongersma, "Plasmonics for extreme light concentration and manipulation," Nat. Mater. **9**(3), 193–204 (2010).
2. D. K. Gramotnev and S. I. Bozhevolnyi, "Plasmonics beyond the diffraction limit," Nat. Photonics **4**(2), 83–91 (2010).
3. E. L. Ru and P. Etchegoin, "Principles of Surface-Enhanced Raman Spectroscopy: and Related Plasmonic Effects," *Elsevier* (2008).
4. M. L. Brongersma, N. J. Halas, and P. Nordlander, "Plasmon-induced hot carrier science and technology," Nat. Nanotechnol. **10**(1), 25–34 (2015).
5. S. Pillai and M. A. Green, "Plasmonics for photovoltaic applications," Sol. Energy Mater. Sol. Cells **94**(9), 1481–1486 (2010).
6. N. S. Mueller, B. G. M. Vieira, D. Höing, F. Schulz, E. B. Barros, H. Lange, and S. Reich, "Direct optical excitation of dark plasmons for hot electron generation," Faraday Discuss. **214**, 159–173 (2019).
7. L. Mingzhao, T.-W. Lee, S. K. Gray, P. Guyot-Sionnest, and M. Pelton, "Excitation of dark plasmons in metal nanoparticles by a localized emitter," Phys. Rev. Lett. **102**(10), 107401 (2009).
8. K. Sakai, T. Yamamoto, and K. Sasaki, "Nanofocusing of structured light for quadrupolar light-matter interactions," Sci. Rep. **8**(1), 7746 (2018).
9. E. Prodan, C. Radloff, N. J. Halas, and P. Nordlander, "A Hybridization Model for the Plasmon Response of Complex Nanostructures," Science **302**(5644), 419–422 (2003).
10. N. S. Mueller, B. G. M. Vieira, F. Schulz, P. Kusch, V. Oddone, E. B. Barros, H. Lange, and S. Reich, "Dark interlayer plasmons in colloidal gold nanoparticle bi-and few-layers," ACS Photonics **5**(10), 3962–3969 (2018).
11. G. Milione, H. I. Sztul, D. A. Nolan, and R. R. Alfano, "Higher-order Poincaré sphere, Stokes parameters, and the angular momentum of light," Phys. Rev. Lett. **107**(5), 053601 (2011).
12. F. Yue, D. Wen, J. Xin, B. D. Gerardot, J. Li, and X. Chen, "Vector Vortex Beam Generation with a Single Plasmonic Metasurface," ACS Photonics **3**(9), 1558–1563 (2016).
13. N. A. Chaitanya, P. Wozniak, P. Banzer, and I. De Leon, "Generation of Vortex Beams using a Plasmonic Quadrumer Nanocluster," in *Conference on Lasers and Electro-Optics*, OSA Technical Digest FM2G.4. (2018).
14. K. Toyoda, K. Miyamoto, N. Aoki, R. Morita, and T. Omatsu, "Using Optical Vortex To Control the Chirality of Twisted Metal Nanostructures," Nano Lett. **12**(7), 3645–3649 (2012).

15. G. Bautista, C. Dreser, X. Zang, D. P. Kern, M. Kauranen, and M. Fleischer, "Collective Effects in Second-Harmonic Generation from Plasmonic Oligomers," Nano Lett. **18**(4), 2571–2580 (2018).
16. J. H. Kang, K. Kim, H. S. Ee, Y. H. Lee, T. Y. Yoon, M. K. Seo, and H. G. Park, "Low-power nano-optical vortex trapping via plasmonic diabolo nanoantennas," Nat. Commun. **2**(1), 582 (2011).
17. R. M. Kerber, J. M. Fitzgerald, S. S. Oh, D. E. Reiter, and O. Hess, "Orbital angular momentum dichroism in nanoantennas," Commun. Phys. **1**(1), 87 (2018).
18. D. K. Sharma, V. Kumar, A. B. Vasista, S. K. Chaubey, and G. V. P. Kumar, "Spin-Hall effect in the scattering of structured light from plasmonic nanowire," Opt. Lett. **43**(11), 2474–2477 (2018).
19. B. Sharma, R. R. Frontiera, A. I. Henry, E. Ringe, and R. P. Van Duyne, "SERS: Materials, applications, and the future," Mater. Today **15**(1-2), 16–25 (2012).
20. M. Hentschel, J. Dorfmüller, H. Giessen, S. Jäger, A. M. Kern, K. Braun, D. Zhang, and A. J. Meixner, "Plasmonic oligomers in cylindrical vector light beams," Beilstein J. Nanotechnol. **4**, 57–65 (2013).
21. A. Yanai, M. Grajower, G. M. Lerman, M. Hentschel, H. Giessen, and U. Levy, "Near- and Far-Field Properties of Plasmonic Oligomers under Radially and Azimuthally Polarized Light Excitation," ACS Nano **8**(5), 4969–4974 (2014).
22. G. H. Yuan, Q. Wang, P. S. Tan, J. Lin, and X.-C. Yuan, "A dynamic plasmonic manipulation technique assisted by phase modulation of an incident optical vortex beam," Nanotechnology **23**(38), 385204 (2012).
23. K. Sakai, T. Yamamoto, and K. Sasaki, "Nanofocusing of structured light for quadrupolar light-matter interactions," Sci. Rep. **8**(1), 7746 (2018).
24. S. Lee, Y. Park, J. Kim, Y. G. Roh, and Q. Park, "Selective bright and dark mode excitation in coupled nanoantennas," Opt. Express **26**(17), 21537–21545 (2018).
25. J. A. Hachtel, S. Y. Cho, R. B. Davidson, M. A. Feldman, M. F. Chisholm, R. F. Haglund, J. C. Idrobo, S. T. Pantelides, and B. J. Lawrie, "Spatially and spectrally resolved orbital angular momentum interactions in plasmonic vortex generators," Light: Sci. Appl. **8**(1), 33 (2019).
26. S. Wang, Z. L. Deng, Y. Cao, D. Hu, Y. Xu, Y. Bao, X. Wang, and X. Li, "Angular Momentum-Dependent Transmission of Circularly Polarized Vortex Beams Through a Plasmonic Coaxial Nanoring," IEEE Photonics J. **10**(1), 1–9 (2018).7
27. D. Naidoo, F. S. Roux, A. Dudley, I. Litvin, B. Piccirillo, L. Marrucci, and A. Forbes, "Controlled generation of higher-order Poincaré sphere beams from a laser," Nat. Photonics **10**(5), 327–332 (2016).
28. P. B. Johnson and R. W. Christy, "Optical constants of the noble metals," Phys. Rev. B **6**(12), 4370–4379 (1972).
29. E. Le Ru and P. Etchegoin, *Principles of surface enhanced Raman spectroscopy: and related plasmonic effects*. (Elsevier Science, New York, 2008).
30. R. W. Yu, L. M. Liz-Marzán, and J. F. Garía de Abajo, "Universal analytical modeling of plasmonic nanoparticles," Chem. Soc. Rev. **46**(22), 6710–6724 (2017).
31. T. J. Davis and D. E. Goméz, "Colloquium: An algebraic model of localized surface plasmons and their interactions," Rev. Mod. Phys. **89**(1), 011003 (2017).
32. N. A. Butakov and J. A. Schuller, "Designing Multipolar Resonances in Dielectric Metamaterials," Sci. Rep. **6**(1), 38487 (2016).
33. C. Forestiere, L. Dal Negro, and G. Miano, "Theory of coupled plasmon modes and Fano-like resonances in subwavelength metal structures," Phys. Rev. B **88**(15), 155411 (2013).
34. U. Hohenester and J. Krenn, "Surface plasmon resonances of single and coupled metallic nanoparticles: A boundary integral method approach," Phys. Rev. B **72**(19), 195429 (2005).
35. S. Reich, N. S. Mueller, and M. Bubula, "Selection Rules for Structured Light in Nanooligomers and Other Nanosystems," ACS Photonics **7**(6), 1537–1550 (2020).
36. I. Teturo, Y. Tanabe, and Y. Onodera. "Group theory and its applications in physics," Springer Science & Business Media 78, (2012).
37. U. Hohenester and A. Trügler, "MNPBEM–A Matlab toolbox for the simulation of plasmonic nanoparticles," Comput. Phys. Commun. **183**(2), 370–381 (2012).
38. J. D Jackson, *Classical Electrodynamics* (Wiley, New York), 3rd ed. (1999).
39. Z. Nir, L. Chuntonov, and G. Haran, "The simplest plasmonic molecules: Metal nanoparticle dimers and trimers," J. Photochem. Photobiol., C **21**, 26–39 (2014).
40. S. Heeg, R. Fernandez-Garcia, A. Oikonomou, F. Schedin, R. Narula, A. A. Maier, and S. Reich, "Polarized plasmonic enhancement by Au nanostructures probed through Raman scattering of suspended graphene," Nano Lett. **13**(1), 301–308 (2013).
41. S. Reich, C. Thomsen, and J. Maultzsch, "Carbon nanotubes: basic concepts and physical properties," John Wiley & Sons (2008).
42. N. I. Bozovic and M. Damnjanovic, "Selection rules for polymers and quasi-one-dimensional crystals. IV. Kronecker products for the line groups isogonal to Dnh," J. Phys. A: Math. Gen. **18**(6), 923–937 (1985).
43. M. Li, H. Fang, X. Li, and X. Yuan, "Exclusive and efficient excitation of plasmonic breathing modes of a metallic nanodisc with the radially polarized optical beams," J. Eur. Opt. Soc.-Rapid Publ. **13**(1), 23 (2017).
44. A. M. Yao and M. J. Padgett, "Orbital angular momentum: origins, behavior and applications," Adv. Opt. Photonics **3**(2), 161–204 (2011).